Integrated tuning fork nanocavity optomechanical transducers with high $f_M Q_M$ product and stress-engineered frequency tuning

R. Zhang,[1] C. Ti,[1] M. I. Davanço,[2] Y. Ren,[1] V. Aksyuk,[2] Y. Liu,[1,2,a)] and K. Srinivasan[2]

[1)] *Department of Mechanical Engineering, Worcester Polytechnic Institute, Worcester, MA 01609, USA*

[2)] *Center for Nanoscale Science and Technology, National Institute of Standards and Technology, Gaithersburg, MD 20899, USA*

(Dated: 18 September 2015)

Cavity optomechanical systems are being widely developed for precision force and displacement measurements. For nanomechanical transducers, there is usually a trade-off between the frequency (f_M) and quality factor (Q_M), which limits temporal resolution and sensitivity. Here, we present a monolithic cavity optomechanical transducer supporting both high f_M and high Q_M. By replacing the common doubly-clamped, Si_3N_4 nanobeam with a tuning fork geometry, we demonstrate devices with the fundamental $f_M \approx 29$ MHz and $Q_M \approx 2.2\times10^5$, corresponding to an $f_M Q_M$ product of 6.35×10^{12} Hz, comparable to the highest values previously demonstrated for room temperature operation. This high $f_M Q_M$ product is partly achieved by engineering the stress of the tuning fork to be 3 times the residual film stress through clamp design, which results in an increase of f_M up to 1.5 times. Simulations reveal that the tuning fork design simultaneously reduces the clamping, thermoelastic dissipation, and intrinsic material damping contributions to mechanical loss. This work may find application when both high temporal and force resolution are important, such as in compact sensors for atomic force microscopy.

Cavity optomechanical systems are being developed for many applications in precision force and displacement measurements[1,2]. Monolithic systems in which nanomechanical transducers are combined with integrated optical readout have been developed in geometries where optical resonances and mechanical modes are co-located within the same physical structure[3–7], and in systems for which optical and mechanical modes are supported by different physical structures and are near-field-coupled[8,9]. Such near-field coupling enables the mechanical resonator size to be scaled down to the nanoscale while maintaining high displacement sensitivity[8,9]in contrast to far-field optical readout, where diffraction effects limit the mechanical resonator size that can be sensitively detected[10]. For a given desired mechanical stiffness (determined by the force sensing application), a nanoscale cantilever can have much higher resonant frequency f_M (and therefore transduction bandwidth/temporal resolution) than a microscale counterpart, due to its smaller effective motional mass (m). Such a high frequency mechanical resonator would ideally exhibit a high mechanical quality factor (Q_M), as the force sensitivity scales as $1/(f_M^{1/2} Q_M^{1/2})$ (Ref. 11). However, there is usually a tradeoff between f_M and Q_M because shrinking down the resonator size comes at the expense of a reduction in Q_M, due to increased clamping losses[11,12]. Here, we demonstrate an integrated silicon nitride cavity optomechanical system where high f_M and Q_M are simultaneously achieved. Using microdisk optical resonators with intrinsic optical quality factor $Q_o > 6\times10^5$ for readout, we develop a doubly-clamped tuning fork geometry as the mechanical resonator, where we take advantage of elastic wave interference to limit the mechanical loss, while retaining the high tensile stress characteristic of stoichiometric Si_3N_4. We investigate different clamp designs that can increase the tensile stress by up to 2.9 times and hence tune f_M on chip, as well as surface treatment to improve Q_M. Devices with $f_M \approx 29$ MHz and $Q_M \approx 2.2\times10^5$ are presented, corresponding to an $f_M Q_M$ product of 6.35×10^{12} Hz.

Doubly-clamped silicon nitride nanobeams have been extensively explored as nanomechanical resonators, with the high residual tensile stress ($\approx$1 GPa) produced by low-pressure chemical vapor deposition (LPCVD) of stoichiometric silicon nitride (Si_3N_4) on silicon enabling $Q_M > 10^6$ to be achieved for MHz frequency modes[13]. In the context of cavity optomechanics, such high-Q_M structures have been evanescently coupled to silica microdisk resonators[8] and incorporated within silicon nitride nanophotonic circuits[14]. Here, our goal is to develop a Si_3N_4 nanobeam-microdisk optomechanical system in which the mechanical frequency f_M is increased to the tens of MHz range while maintaining high Q_M. To do so, we replace the commonly used single beam resonator with a tuning fork mechanical resonator, as shown in Fig. 1(a).

For nanomechanical resonators operating in vacuum, there are several sources of mechanical energy dissipation: clamping losses (Q_{clamp}), thermoelastic dissipation (TED) (Q_{TED}), and material losses (Q_{mat}). The total mechanical quality factor Q_M can then be written as $1/Q_M = 1/Q_{clamp} + 1/Q_{TED} + 1/Q_{mat} + 1/Q_{other}$ (Ref. 11). Clamping losses occur when the elastic energy radiates into its support structures[11,15]. TED is the energy dissipation due to strain-induced heating and the resulting temperature gradients[16,17], and is expected to

[a)]Electronic mail: yliu11@wpi.edu

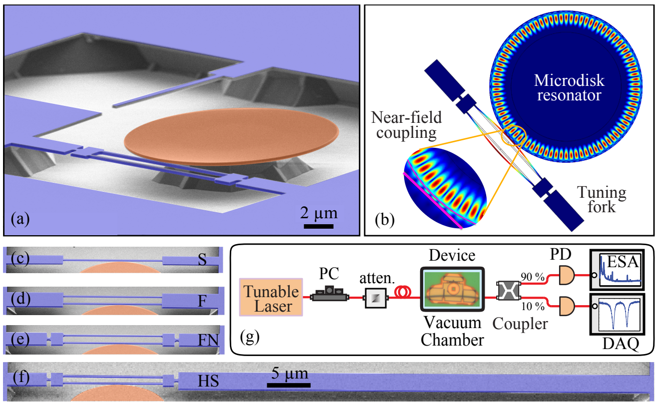

FIG. 1. (a) False-colored scanning electron micrograph (SEM) of a fabricated device. The orange region indicates the Si_3N_4 microdisk optical resonator while the blue region indicates the mechanical resonator and supporting structures. (b) Working principle of the device. The colored tuning fork shows the calculated mode shape of the first-order, in-plane, out-of-phase mechanical mode. The colored disk shows the $TE_{1,43}$ whispering gallery optical mode. (c)-(f) SEM images of four different mechanical resonator designs: (c) single beam (S), (d) tuning fork (F), (e) tuning fork with neck (FN), (f) high-stress tuning fork (HS). (g) Schematic of the characterization system. PC, polarization controller; PD, photodiode; DAQ, data acquisition; ESA, electrical spectrum analyzer.

dominate Akhesier damping for devices with our geometry/aspect ratios (so that the latter is not considered further in our discussion)[18]. In addition, losses caused by localized defect states both on the surface and in the volume of the material cannot be neglected[18]. Compared with the modes of single cantilever devices[8,9,14] the in-plane, out-of-phase mechanical mode of the tuning fork structure (mode shape shown in Fig. 1(b)) enables the total force and moment at the outer end of the clamps to be zero. Therefore, the motion of the beams is effectively decoupled from the clamps, resulting in an expected lower clamping losses. This effect, which has been used in a variety of mechanical structures ranging from clocks and musical instruments (the tuning fork was invented in 1711[19]) to atomic force microscope sensors[20], can also be understood as destructive interference of elastic waves, and similar ideas have been implemented in double disk cavity optomechanical structures[21] as well as incorporated within silicon photonic crystal cavities[22]. In contrast to those structures, the doubly clamped geometry we adopt (Fig. 1(a)-(b)) maintains the high residual tensile stress of the Si_3N_4 film, which is important for maintaining high f_M and Q_M[12].

To verify these benefits of the design, we fabricated cavity optomechanical transducers with four types of mechanical resonators: single beams (S), turning forks (F), and tuning forks with necks (FN), as shown in Fig. 1(c)-(e). The tuning fork with and without neck geometries are nearly identical, with only the specifics of the clamping geometry slightly modified by inserting a neck region. Each mechanical resonator was coupled to a microdisk optical resonator that is 15 μm in diameter, and the separation between the optical and mechanical resonators is 150 nm. The devices were fabricated in a 250 nm stoichiometric silicon nitride film with an internal tensile stress of $\approx$ 1.1 GPa, using electron-beam lithography and dry etching processes similar to our previous work on high-Q Si_3N_4 microdisk optomechanical resonators[23]. The mechanical resonator beams are 150 nm wide, and the beam lengths are varied between 12 μm and 40 μm to investigate the dependence of device performance on the beam length. Stress tuning is an effective way to increase both f_M and Q_M, and stress tuning of chip-based devices was previously realized by substrate bending[12]. In the tuning fork design, a stress level within the mechanical resonator above that of the deposited film was achieved by increasing the clamp length on one side of the fork, for example, by 100 μm as shown in Fig. 1(f). Due to the initial unbalanced tensile forces in the clamp and beam (details available in supplementary materials[24]), the stress is redistributed after undercut, such that it decreases in the wide suspended clamp and increases by up to 3 times[24] in the attached narrow beams of the tuning fork. We note that the stress tuning has been achieved by a design-enabled, on-chip approach, with no additional process needed after the device fabrication. This stress tuning method provides more flexibility and better control of engineering f_M of nanomechanical resonators.

For each mechanical resonator geometry shown in Fig. 1(c)-(f), devices with three different beam lengths (12 μm, 20 μm, and 40 μm) were fabricated and characterized in vacuum (0.13 Pa) in order to evaluate both their f_M and Q_M. The characterization setup is shown in Fig. 1(g), with more details available in the supplementary material[24]. The typical optical quality factor Q_o is $> 10^5$, as shown in Fig. 2(a). The optomechanical coupling coefficient ($g_{OM}/2\pi$) of our device is calculated to be 140 MHz/nm by perturbation theory[25] using finite element method (FEM) determined mode solutions (Fig. 1(b)), with details provided in the supplementary

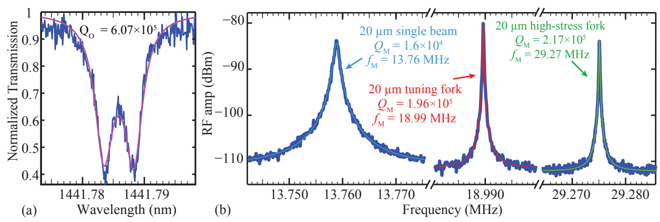

FIG. 2. (a) Typical optical spectrum of microdisk resonator. The intrinsic optical Q factor is $6.07\times10^5 \pm 6\times10^3$. The 95 % confidence interval range for Q_o is determined by a nonlinear least squares fit to the data. (b) Mechanical spectra of a single beam, tuning fork, and high-stress tuning fork structures with 20 μm beam length. The 95 % confidence intervals for Q_M from the curve fitting are typically $\pm$3 %, and are summarized in Fig. 3(a)-(b).

material[24]. Figure 2(b) shows the measured mechanical spectra of devices with the same beam length (20 μm) but different geometries. We find that the tuning fork with and without neck increase Q_M by 12 times and f_M by 1.4 times the values of a single beam structure, respectively. The high-stress tuning fork device with a longer clamp produces an even more pronounced increase in Q_M and f_M, by 13.5 times and 2.1 times the values of a single beam structure, respectively. The stress-tuning induced f_M increase is 1.5 times compared with regular tuning forks. We note that this device exhibited the highest $f_M Q_M$ product (6.35×10^{12} Hz) for any of the structures we have investigated.

The thermomechanical force noise is also decreased using the tuning fork geometry. Assuming the force noise is frequency independent, its spectral density can be estimated by $S_F = 4kk_BT/(2\pi f_M Q_M)$ (Ref. 11), where k is the cantilever effective spring constant, k_B the Boltzmann constant, and T the temperature. For 20 μm long single beam, fork, and high-stress fork devices, the FEM calculated k are 13.23 N/m, 26.27 N/m, and 60.58 N/m, respectively. Using the calculated k values and the measured f_M and Q_M values, the corresponding $S_F^{1/2}$ are 0.40 fN/Hz$^{1/2}$, 0.14 fN/Hz$^{1/2}$ and 0.16 fN/Hz$^{1/2}$, respectively. These results show that, although k is increased by the tuning fork design, the high $f_M Q_M$ product still reduces the force noise by a factor of $\approx$2.9 compared with the single beam devices. We also note that the mechanical damping coefficient $\gamma = k/(2\pi m f_M Q_M)$ and the corresponding thermodynamic force noise $S_F = 4k_BTm\gamma$ do not further decrease by the high stress tuning fork, which introduces an additional stress increase of 2.3 times compared with regular fork[24], as the increase in $f_M Q_M$ is offset by the increase in k.

The full parametric study of single beam, tuning fork, and tuning fork with neck structures is shown in Fig. 3, where the labels P1, P2, and P3 indicate experimental results from different batches of devices. Both the experimentally measured and FEM simulated f_M values are shown in Fig. 3(a). In the experiment, two fundamental in-plane modes, one in-phase and one out-of-phase were observed with frequencies close to the simulated values. The higher frequency one was determined to be the out-of-phase mode, due to the higher effective stiffness resulting from the mode being decoupled from the clamps. The next observed resonances were $\approx$ 50 % higher in frequency, and correspond to higher-order in-plane modes, while out-of-plane modes were not observed due to negligible optomechanical coupling. Fig. 3(a) further shows that the measured f_M is higher in the tuning fork device architectures compared to single-beam devices for all beam lengths. This confirms that the tuning fork structure helps to decouple motion of the beams from the clamps, which effectively increases the clamp stiffness.

According to Fig. 3(b), the tuning fork design helps to increase Q_M for all the beam lengths in the experiment. We believe the reduction of clamping losses is one of the primary reasons for the experimentally measured Q_M improvements, based on the following discussion. First, we plot measured Q_M values for both the out-of-phase and in-phase mechanical modes for the tuning fork structure in Fig. 4(a). In all the cases, the out-of-phase modes have higher Q_M values than the corresponding in-phase modes, which is expected because the in-phase modes do not produce destructive elastic wave interference in the clamping regions. Next, we note that the tuning fork design is more effective in achieving increased Q_M in devices with shorter beams. This is because the fraction of the modal mechanical energy within the clamping regions is comparatively smaller for longer beams, so that for long enough beams, clamping loss is likely no longer a dominant loss mechanism[15]. We also fabricated devices with 80 μm long beams (data not shown), with measured Q_M comparable to the 40 μm devices. We note that very little difference is seen in the experiments between the f_M and Q_M values of the tuning forks with and without neck, indicating that the energy dissipation reduction is essentially the same for both.

In addition to the clamping losses, we also consider whether the TED contribution to Q_M may be improved by the tuning fork geometries, using FEM simulations in which material deformation is coupled to temperature gradients[24]. Indeed, we do find that the TED contribution in tuning fork devices is smaller than that in single-beam ones for all beam lengths, as shown in Fig. 3(b). Simulation results of the local temperature gradient are shown in Fig. 3(c). The localized deformation in the tuning fork structure helps to decrease the deformation-induced heating and cooling areas. Therefore, the heat flows driven by the temperature gradient become smaller in the tuning fork structure, which results in lower TED than that of the single-beam structure. In addition, calculation of TED for both the out-of-phase and in-phase modes in tuning fork geometry (Fig. 4(a)) confirms that the out-of-phase modes have lower TED. However, the TED improvements in simulation are much smaller than the total loss improvements observed in the experiment, which indicates that the Q_M improvements are not mainly due to decreased TED.

To simulate the effect of material losses, similar to a previously published work[18], we introduce an additional imaginary part to the Si_3N_4 Youngs modulus, so that it becomes $E = E_1 + iE_2$, and determine the resulting quality factor Q_{mat} from finite element simulations. Under the assumption that $(1/Q_{clamp} + 1/Q_{other})$ is small in the tuning fork geometries, we choose a value of $E_2 = 20$ MPa ($E_1 = 290$ GPa) to achieve a reasonable agreement between experimental losses and simulated $(1/Q_{TED} + 1/Q_{mat})$ for the tuning fork devices. This single choice of E_2 is consistent with the literature[26] and results in losses that do not exceed the experimentally measured total losses for any of the devices. The simulation results show that the tuning fork structure helps to decrease the damping due to the material defect losses ($1/Q_{mat}$) in addition to decreasing the clamping losses. This can be explained by the simulated elastic

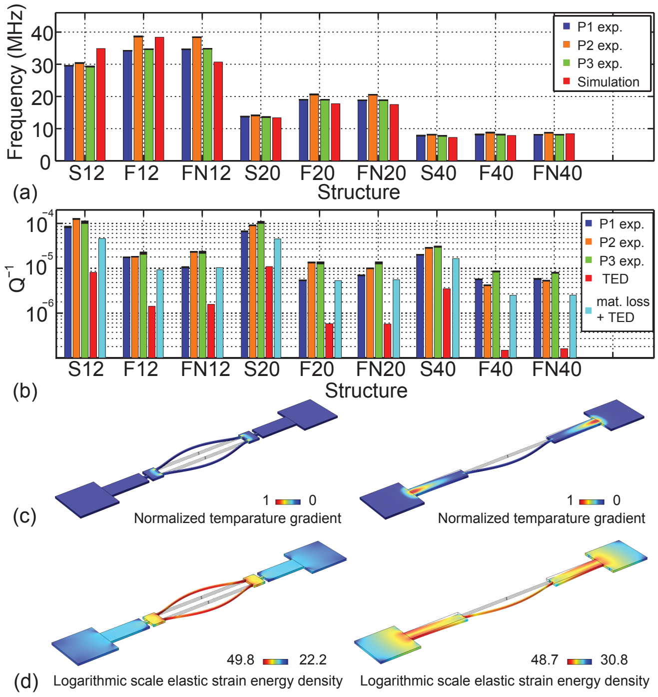

FIG. 3. (a) FEM calculated and experimentally measured frequencies of the mechanical resonators, where the labels P1, P2, and P3 indicate experimental results from different batches of devices. The horizontal axis labels S, F, and FN stand for single beam, tuning fork, and tuning fork with neck, respectively, while 12, 20, and 40 specify the beam length in micrometers. (b) Experimentally measured Q_M^{-1}, FEM calculated Q_{TED}^{-1}, and FEM calculated $Q_{TED}^{-1} + Q_{mat}^{-1}$. The 95 % confidence interval ranges for f_M and Q_M, determined by a nonlinear least squares fit to the data, are denoted by the solid black regions above each bar in the graphs. (c) FEM calculated normalized temperature gradient for tuning fork and single beam structures during vibration. (d) FEM calculated elastic strain energy density on a logarithmic scale for tuning fork and single beam structures during vibration.

energy density shown in Fig. 3(d), corresponding to the strain distribution during vibration. The deformation of the tuning fork structures is more localized in the center beam region, while the deformation in single beam structures is distributed in both beams and clamps. With a smaller amount of deformed material, damping due to material loss is reduced in tuning fork structures.

As shown in Fig. 3(b), differences between experimentally measured $1/Q_M$ and simulated $(1/Q_{TED}+1/Q_{mat})$ of single beam devices are much larger than those of the tuning fork devices, especially for shorter length beams, indicating higher clamping losses for single beam structures. In total, we believe the clamping loss, damping due to material loss, and TED are all reduced in the tuning fork structure, through localized deformation resulting from elastic wave interference.

From the characterization we also noticed that although they are nominally the same structures, samples from chip P3 have lower Q_M than those from other batches. We briefly consider whether this is due to surface losses, which are parts of the material losses. Such losses are caused by the friction processes resulting from surface defects and roughness[27,28] and have been viewed as a potentially universal limiting loss mechanism in Si_3N_4 nanomechanical resonators[29], might be reduced in our structures via surface treatment. We immersed the P3 devices into 1:10 hydrofluoric acid: water (HF:H_2O) for 90 s to remove a thin layer of material that may have been damaged during the dry etching process. According to Fig. 4(b), Q_M for all of the devices on this sample were improved by up to 2 times after the HF treatment, approaching (but not exceeding) the highest values we have achieved in untreated samples (shown in Fig. 2). Further investigation is needed to determine whether a surface treatment can be applied to yield higher Q_M values than the best untreated samples.

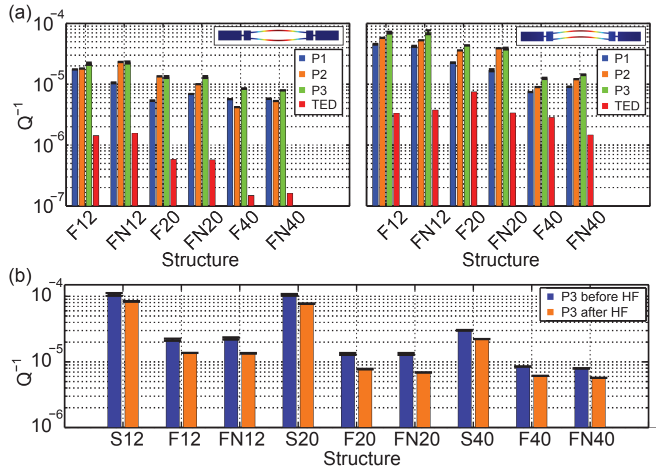

FIG. 4. (a) Experimentally measured Q_M^{-1} and FEM calculated Q_{TED}^{-1} for out-of-phase (left) and in-phase (right) mechanical modes. The FEM calculated mode shapes are also shown in the insets. (b) Experimentally measured Q_M^{-1} before and after HF treatment. The 95 % confidence interval ranges for f_M and Q_M, determined by a nonlinear least squares fit to the data, are denoted by the error bars in the graphs. Some of the error bars are smaller than the bar graph line widths.

In conclusion, we have developed silicon nitride tuning fork cavity optomechanical transducers. These structures simultaneously increase the resonant frequency (f_M) and mechanical quality factor (Q_M) of the fundamental mechanical mode compared with single beam devices, by up to 1.4 times and 12 times, respectively, through an effective increase in the clamp stiffness and reduction in energy dissipation. By engineering the clamp geometry further, calculation indicates that we increase the tensile stress in the beams by 2.9 times compared with the intrinsic stress of the Si_3N_4 film, resulting in an experimentally measured frequency increase of 1.5 compared with that of the regular tuning fork, while the mechanical damping remained unchanged. The highest measured $f_M Q_M$ product of 6.35×10^{12} Hz at room temperature is on par with the highest values reported for doubly-clamped Si_3N_4 beams. This tuning fork design with both high Q_M and high f_M can find applications in force sensing applications, including those that use active feedback cooling to damp mechanical motion[30,31].

The authors acknowledge Dr. Alexander Grey Krause from Delft University of Technology in the Netherlands for helpful discussion.

[1] T. J. Kippenberg and K. J. Vahala, Science **321**, 1172 (2008).
[2] M. Metcalfe, Applied Physics Reviews **1**, 031105 (2014).
[3] T. Antoni, A. G. Kuhn, T. Briant, P.-F. Cohadon, A. Heidmann, R. Braive, A. Beveratos, I. Abram, L. L. Gratiet, I. Sagnes, *et al.*, Optics Letters **36**, 3434 (2011).
[4] M. Eichenfield, R. Camacho, J. Chan, K. J. Vahala, and O. Painter, Nature **459**, 550 (2009).
[5] S. Forstner, S. Prams, J. Knittel, E. D. van Ooijen, J. D. Swaim, G. I. Harris, A. Szorkovszky, W. P. Bowen, and H. Rubinsztein-Dunlop, Phys. Rev. Lett. **108**, 120801 (2012).
[6] K. H. Kim, G. Bahl, W. Lee, J. Liu, M. Tomes, X. Fan, and T. Carmon, Light: Science & Applications **2**, e110 (2013).
[7] M. Wu, A. C. Hryciw, C. Healey, D. P. Lake, H. Jayakumar, M. R. Freeman, J. P. Davis, and P. E. Barclay, Physical Review X **4**, 021052 (2014).
[8] E. Gavartin, P. Verlot, and T. J. Kippenberg, Nature Nanotechnology **7**, 509 (2012).
[9] Y. Liu, H. Miao, V. Aksyuk, and K. Srinivasan, Optics Express **20**, 18268 (2012).
[10] T. Kouh, D. Karabacak, D. H. Kim, and K. L. Ekinci, Appl. Phys. Lett. **86**, 013106 (2005).
[11] K. Y. Yasumura, T. D. Stowe, E. M. Chow, T. Pfafman, T. W. Kenny, B. C. Stipe, and D. Rugar, Microelectromechanical Systems, Journal of **9**, 117 (2000).
[12] S. S. Verbridge, D. F. Shapiro, H. G. Craighead, and J. M. Parpia, Nano Letters **7**, 1728 (2007).
[13] S. S. Verbridge, H. G. Craighead, and J. M. Parpia, Applied Physics Letters **92**, 013112 (2008).
[14] K. Y. Fong, W. H. P. Pernice, M. Li, and H. X. Tang, Applied Physics Letters **97**, 073112 (2010).
[15] Z. Hao, A. Erbil, and F. Ayazi, Sensors and Actuators A: Physical **109**, 156 (2003).
[16] A. Duwel, R. N. Candler, T. W. Kenny, and M. Varghese, Microelectromechanical Systems, Journal of **15**, 1437 (2006).
[17] R. Lifshitz and M. L. Roukes, Physical review B **61**, 5600 (2000).
[18] Q. P. Unterreithmeier, T. Faust, and J. P. Kotthaus, Physical review letters **105**, 027205 (2010).
[19] H. Feldmann, Laryngo-rhino-otologie **76**, 116 (1997).
[20] F. Giessibl, Reviews of Modern Physics **75**, 949 (2003).
[21] M. Zhang, G. Luiz, S. Shah, G. Wiederhecker, and M. Lipson, Applied Physics Letters **105**, 051904 (2014).
[22] X. Sun, J. Zheng, M. Poot, C. W. Wong, and H. X. Tang, Nano Letters **12**, 2299 (2012).
[23] Y. Liu, M. Davanço, V. Aksyuk, and K. Srinivasan, Phys. Rev. Lett. **110**, 223603 (2013).
[24] See supplemental material at [URL] for details on fabrication, characterization setup, and FEM simulations.
[25] M. Eichenfield, J. Chan, R. M. Camacho, K. J. Vahala, and O. Painter, Nature **462**, 78 (2009).
[26] S. Schmid, K. Jensen, K. Nielsen, and A. Boisen, Physical Review B **84**, 165307 (2011).
[27] M. Imboden and P. Mohanty, Physics Reports **534**, 89 (2014).
[28] C. Seoánez, F. Guinea, and A. C. Neto, Physical Review B **77**, 125107 (2008).
[29] L. G. Villanueva and S. Schmid, Physical review letters **113**, 227201 (2014).
[30] D. Wilson, V. Sudhir, N. Piro, R. Schilling, A. Ghadimi, and T. Kippenberg, arXiv preprint arXiv:1410.6191 (2014).
[31] A. G. Krause, T. D. Blasius, and O. Painter, arXiv preprint arXiv:1506.01249 (2015)
.